Available online at www.sciencedirect.com

ScienceDirect

journal homepage: www.elsevier.com/locate/issn/15375110

Research Paper

# Determination of overall heat transfer coefficient for greenhouse energy-saving screen using Trnsys and hotbox

Anis Rabiu [a], Wook-Ho Na [b], Timothy Denen Akpenpuun [c], Adnan Rasheed [b], Misbaudeen Aderemi Adesanya [a], Qazeem Opeyemi Ogunlowo [a], Hyeon Tae Kim [d], Hyun-Woo Lee [a,b,*]

[a] Department of Agricultural Civil Engineering, College of Agricultural and Life Sciences, Kyungpook National University, Daegu 702-701, South Korea
[b] Smart Agriculture Innovation Centre, Kyungpook National University, Daegu 41566, South Korea
[c] Department of Agricultural and Biosystems Engineering, University of Ilorin, PMB 1515, Ilorin, Nigeria
[d] Department of Bio-Industrial Machinery Engineering, Gyeongsang National University, Jinju 52828, South Korea

ARTICLE INFO

*Article history:*
Received 28 July 2021
Received in revised form
25 February 2022
Accepted 8 March 2022

*Keywords:*
Thermal screen
Permeability
Airflow
TRNSYS
Hotbox

The high energy consumption in the greenhouse during the winter season necessitates the development of various thermal screens for energy-saving purposes. However, there is limited data on the precise properties of thermal screens, while little research has investigated a methodological approach for measuring the screen's energy-saving capacity for greenhouse energy efficiency. This research aims to determine the thermophysical, radiative, and aerodynamic properties of selected commercial greenhouse thermal screens. The transient system simulation (TRNSYS) model was used to simulate the heat flux and derive the thermal retention qualities of the thermal screens through their measured properties. The model was validated by comparing the simulated and experimental heat transfer coefficients, expressed as the overall heat transfer coefficient (U-value), thereby determining the thermal retention of the screens. In addition, the simulated U-value was compared to the experimental U-value in material permeability to investigate the influence of screen porosity on heat loss. The statistical analysis t-test was conducted to compare the U-values obtained from the simulation and the experimental hotbox. The simulated U-values (for computed permeability) indicated that samples M1 and M3 exhibited the lowest U-value of 4.4 W $m^{-2}$ $K^{-1}$, while white polyester, Luxous, PH-super, PH-66, M2, Clima45 (0), and New-Lux showed higher U-values of 82%, 105%, 161%, 123%, 41%, 102%, and 118%, respectively. Because of their low material porosity, M1, M2, and M3 samples showed better greenhouse thermal retention over others. Conclusively, the permeability features of the greenhouse energy screen materials have a substantial impact on their U-values.



* *Corresponding author*. Department of Agricultural Civil Engineering, College of Agricultural and Life Sciences, Kyungpook National University, Daegu 702-701, South Korea.
E-mail addresses: rabiuanis@gmail.com (A. Rabiu), Wooks121@hanmail.net (W.-H. Na), akpenpuun.td@unilorin.edu.ng (T.D. Akpenpuun), adnan.upm.spain@gmail.com (A. Rasheed), misbauadesanya@gmail.com (M.A. Adesanya), cosmosopy@yahoo.com (Q.O. Ogunlowo), bioani@gnu.ac.kr (H.T. Kim), whlee@knu.ac.kr (H.-W. Lee).
https://doi.org/10.1016/j.biosystemseng.2022.03.002
1537-5110/

**Nomenclature**

Symbols

| | |
|---|---|
| A | Cross-sectional area of the sample, $m^2$ |
| ACH | Air change per hour, $h^{-1}$ |
| $C_{cover}$ | Cloudiness factor of the sky |
| Cp | Specific heat capacity of air, kJ $K^{-1}$ $kg^{-1}$ |
| $dP$ | Differential pressure, Pa |
| $E_s$ | The emissive power of the thermal screen, W $m^{-2}$ |
| $f_{s,sky}$ | Fraction of the sky seen by the outside surface |
| $H_e$ | External convective heat transfer coefficient, W $m^{-2}K^{-1}$ |
| K | Permeability of the thermal screen, $m^2$ |
| $K_t$ | Flow coefficient of the screen sample, $m^3$ $m^{-2}$ $s^{-1}$. $Pa^{-0.66}$ |
| L | Thickness of the Hotbox, m |
| $\Delta P_r$ | Reference pressure difference, Pa |
| $Q_{conv}$ | Convective heat loss to the surface, W |
| $Q_{rad}$ | Radiative heat loss to the surface, W |
| Q | Heat loss through the thermal screen, W |
| $Q_{loss}$ | Total heat loss by the hotbox model, W |
| $Q_{inf}$ | Heat loss through the screen pore, W |
| $Q_a$ | Inward sky radiation toward the thermal screen, W $m^{-2}$ |
| $Q_b$ | Upward radiation from the thermal screens to the sky, W $m^{-2}$ |
| $Q_c$ | Upward longwave radiation from the thermal screen toward the black fabric, W $m^{-2}$ |
| $Q_d$ | Inward longwave radiation toward the thermal screen from the black fabric, W $m^{-2}$ |
| $Q_{frate}$ | Infiltration airflow rate through the screen per unit area, $m^3$ $h^{-1}$ $m^{-2}$ |
| $Q_r$ | Heating power of the heater, W |
| $Q_w$ | Heat losses through the hotbox surfaces, W |
| $S_a$ | Sky downward shortwave radiation, W $m^{-2}$ |
| $S_b$ | Outward shortwave radiation toward the sky from the thermal screen, W $m^{-2}$ |
| $S_c$ | Outward shortwave radiation from the thermal screen toward the black fabric, W $m^{-2}$ |
| $S_d$ | Shortwave radiation from the black fabric toward the thermal screen, W $m^{-2}$ |
| $S_w$ | Surface area, $m^2$ |
| $T_a$ | Ambient temperature, °C |
| $T_i$ | Inside air temperature, °C |
| $T_{is}$ | Internal surface temperature, °C |
| $T_{es}$ | External surface temperature, °C |
| $T_{fsky}$ | Fictive sky temperature used for longwave radiation, °C |
| $T_{grd}$ | Fictive ground temperature used for longwave radiation, °C |
| $T_{sky}$ | Effective sky temperature, °C |
| $u$ | Velocity, m $s^{-1}$ |
| U | Overall heat transfer coefficient, W $m^{-2}K^{-1}$ |
| $U_{avg}^{exp}$ | Average experimental U-value result, W $m^{-2}K^{-1}$ |
| $U_i^{exp}$ | Experimental U-value result, W $m^{-2}K^{-1}$ |
| $U_i^{sim}$ | Simulation U-value result, W $m^{-2}$ $K^{-1}$ |
| v | Ambient wind speed, m $s^{-1}$ |
| V | Airflow rate, $m^3$ $s^{-1}$ |
| X | Thickness of the thermal screen, m |

Greek symbols

| | |
|---|---|
| $\alpha_L$ | Longwave absorptivity of the thermal screen |
| $\varepsilon_b$ | Emittance of black fabric |
| $\varepsilon_0$ | Emittance of the clear sky |
| $\lambda$ | Thermal conductivity of the polystyrene insulation, W $m^{-1}$ $K^{-1}$ |
| $\mu$ | Denotes $10^{-6}$ |
| $\mu_d$ | Dynamic viscosity of air, Pa. s |
| $\rho$ | Air density, $kg.m^{-3}$ |
| $\rho_b$ | Reflectance of black fabric |
| $\rho_L$ | Longwave reflectance of the thermal screen |
| $\rho_s$ | Reflectance of the thermal screen |
| $\sigma$ | Stephan–Boltzmann constant |
| $\tau_b$ | Transmittance of black fabric |
| $\tau_L$ | Longwave transmittance of the thermal screen |
| $\tau_S$ | Transmittance of the thermal screen |

Abbreviations

| | |
|---|---|
| ASHRAE | American Society of Heating, Refrigerating and Air-conditioning |
| BES | Building energy simulation |
| KMA | Korean Metrological Administration |
| LBNL | Lawrence Berkeley National Laboratory |
| PE | Polyethylene |
| QTM-500 | Quick thermal meter |
| TRNSYS | Transient system simulation |

## 1. Introduction

The continuous global population growth has led to an exponential rise in the food demand with controlled environmental agriculture, such as a greenhouse providing alternative favourable conditions for crop cultivation all year round. Greenhouse farming is one of the most common approaches, creating a satisfactory microclimate for crop growth. This cultivation strategy is cost-effective and meets global food security and environmental sustainability (Ouazzani Chahidi et al., 2021). However, the greenhouse is the most energy-intensive sector in the commercial agriculture industry (Zhang et al., 2020). For instance, in South Korea, the greenhouse-heating energy requirement during winter was estimated to be 40% of the total production cost (Rasheed et al., 2018b). Therefore, the high energy consumption has prompted innovative solutions and technology to promote energy savings without compromising crop growth (Yano & Cossu, 2019). According to previous studies, numerous energy-saving techniques and strategies have been applied to decrease the operating cost by reducing the greenhouse-heating demand during the winter season (Cuce et al., 2016).

The energy simulation tools have successfully predicted the greenhouse thermal behaviour and performance by analysing the energy requirements and energy-efficient screens to mitigate the high heating demand and reduce the operating cost (Yano & Cossu, 2019). The persistently high energy demand has been the primary concern of the greenhouse growers, researchers, and practitioners (Teitel et al., 2009; Rasheed et al., 2018b; Yano & Cossu, 2019), thus it must be duly managed and optimised to maintain the most favourable environment for optimum plant growth, enabling economical production in winter (Akpenpuun et al., 2021).

Among the several techniques to reduce the heating demand and improve energy retention inside the greenhouse, thermal screens reduced the night time heat loss by about 40%–70% night time (Ahamed et al., 2019) and saved about 23%–60% heating energy by reducing the heated air in the greenhouse microenvironment (Ahamed et al., 2019). Thermal screens act as a blanket (insulation material) preventing heat loss to the ambient environment at nighttime (Frangi, Piatti, & Amoroso, 2011), and their energy-saving performance is influenced by the location and types of screens used (De Zwart, 1996). Abu Bakar et al. (2015) and Rasheed et al. (2018a) reported that greenhouse design parameters, construction materials, type and number of energy screens significantly affect the heating consumption and consequently, the energy demand in the greenhouse. Therefore, the thermal performance of the energy-saving screens is required to improve greenhouse insulation (Vitoshkin et al. 2019), while the overall heat transfer coefficient (U-value) can determine the thermal capacity of screen materials (Rasheed et al., 2018c). According to Rasheed et al. (2018c), many novel thermal screens are available in the South Korean market, possessing unidentified properties, thus making it challenging for the grower to select the materials with optimal energy-saving characteristics. However, comprehensive information about the U-value could facilitate an intelligent economic investment in suitable energy-saving thermal screens, thereby reducing the initial cost of production (Baeza et al., 2020). Moreover, U-value and other essential information on the screen materials could enable the manufacturer to fabricate the best suited materials for the greenhouse (Hemming et al., 2017).

Geoola et al. (2009) constructed a guarded hotbox to test the influence of temperature difference and wind velocity on the overall heat transfer coefficient of greenhouse polyethylene plastic sheets, with or without thermal screen under various conditions. Diop et al. (2012) developed a guarded hotbox to determine the U-value of greenhouse covering materials and thermal screens concurrently, with and without shelter from sky radiation. Furthermore, Lu and Memari (2018) performed a comparative study of building enclosure testing laboratory hotbox to evaluate the thermal properties of the building envelope systems. This study was further performed using dynamic models, including Anderlind's regression and R–C network models and validated the results using the hotbox test method (Lu & Memari, 2018). Rasheed et al. (2018a) created a hotbox building energy simulation (BES) model to compute the U-value of polyethylene, polycarbonate, polyvinyl chloride, and horticultural glass. The study considered all examined materials as impermeable without any aerodynamic properties, accounting for the heat loss through the pores (Rasheed et al., 2018a). Furthermore, Rasheed et al. (2018a) used the hotbox BES model to study the U-value of several selected greenhouse thermal screens under well-defined climatic conditions to investigate their thermal performances. However, only a few studies consider the aerodynamic properties (airflow characteristics and permeability) of thermal screens in the models to predict the energy retention capabilities of the screen materials. Miguel et al. (1997) investigated the airflow properties of nine different thermal, shade, and insect greenhouse screens using Forcheimer's equation and Darcy's formula to determine their porosities and permeabilities. The experiments revealed that the permeability of thermal screens is around $10^{-11}$ $m^2$, which can increase up to 3.5 times due to damage from poor handling. Castellano et al. (2016) used a laboratory macro wind tunnel to determine the aerodynamic and geometric parameters of 15 greenhouse net screens. The study established the airflow rate and pressure-drop curves with a velocity less than 4 m $s^{-1}$ using Bernoulli's principle of the loss coefficient. Further, Valera et al. (2006) used air-suction and wind tunnel systems to evaluate the flow resistance, permeability, and inertial factors of chosen greenhouse nets as a function of porosity. They reported that the screen porosities ranged from 0.29 to 0.48, and a second-order polynomial was used to describe the relationship between inertial-factor and porosity.

In recent times, dynamic simulation software's have been introduced in the greenhouse research to address the thermal phenomena. However, transient system simulation (TRNSYS), a BES used to study thermal systems, estimate energy load, and analyse energy management of a greenhouse microclimate for effective economic efficiency (Rasheed et al., 2015; Ahamed et al., 2020). TRNSYS is a versatile software, also used in commercial, industrial, and domestic buildings. Furthermore, the software applications have been extended to the agricultural sector, modelling a real-life scenario, including processing dynamic weather data, solar radiation, building orientation and geometry, energy storage system, ventilation, HVAC, and renewable energy (Baglivo et al., 2020). The TRNSYS tool can model a thermal system to determine the hourly, daily, and yearly energy demands based on the input parameters (Rasheed et al., 2015; Choab et al., 2021). Moreover, several studies have applied the TRNSYS model to simulate the greenhouse microclimates and analyse the energy management (Ahamed et al., 2020; Baglivo et al., 2020; Mashonjowa et al., 2013; Rasheed et al., 2018b, 2020a). Ahamed et al. (2020) used TRNSYS to predict the heating requirements of a Chinese-style solar greenhouse for Canadian prairies, making several assumptions regarding thermal screens due to the unavailability of specific features in the TRNBuild library, required for the greenhouse model simulations. However, using the actual screen properties reduces the model uncertainty while predicting the energy loads. Similarly, Rasheed et al. (2020) used TRNSYS to simulate the microclimate of a multi-span greenhouse, considering the daily and annual controls of screens, roof vents, and heating setpoints in favour of the crop demand (Rasheed et al. 2020). The study examined the effects of greenhouse design parameters, including natural ventilation, number of screens, double glazing, north–wall insulation, roof geometry, covering materials, heating

setpoint controls, and thermal screens on the maximum-heating load. However, little attention was laid on the thermal screen airflow characteristics, accounting for the heat loss through the screen pores when used for energy saving.

Studies have reported the properties of greenhouse screens of several material configurations in regards to permeability (Miguel, 1998; López et al., 2016; Hemming et al., 2017; Hung Anh & Pásztory, 2021), radiometric property (Abdel-Ghany et al., 2015; Rafiq, 2019), and thermal radiation (Balemans, 1989; Papadakis et al., 2000; Andersson, 2010; Rafiq et al., 2019). However, the properties were separately used, ignoring their cumulative effect on the screen thermal performance. The ability of thermal screens to diffuse, emit, and reflect the solar spectrum or longwave radiation into the greenhouse environment depends on their material compositions and structures, making a single thermal screen practically nonideal for all crops, locations, and seasonal weather variations (Baeza et al., 2020). Therefore, the combined properties of thermal screens must be utilised by an energy simulation software to determine the greenhouse energy demand.

Hitherto, Hemming et al. (2017) examined thermal and shading screens with KASPRO software to investigate their energy-saving capabilities. Their study considered the screen radiation exchange, humidity transfer, air permeability of woven and knitted textiles or foils, open and closed structures, diffusion, aluminised transparent, and colour of various screens. Their investigation was based on the radiation exchange, including transmissivity and emissivity of longwave radiation. Baneshi et al. (2020) developed a greenhouse model in MATLAB to simulate cultivation microclimate and measure the spectral radiative properties of some greenhouse covering materials in a wide wavelength range from 0.2 to 28 μm. The authors concluded that appropriate covering plastic reduces the annual cooling and heating loads by 9.8% and 6.3%, respectively. Hence, this study revealed insufficient data about the specific spectral radiative properties of greenhouse plastic screen (Baneshi et al., 2020), and limited information about the thermal performance of thermal screens are available to growers to meet specific crop requirements (Rafiq et al., 2020). Rafiq et al. (2019) investigated the properties of thermal screens under natural conditions and reported the emissivity values of PE, LD-13, LD-15, and PH-20 materials as 0.439 ± 0.020, 0.460 ± 0.010, 0.454 ± 0.010, and 0.499 ± 0.006, respectively. Abdel-Ghany et al. (2015) determined shortwave and longwave radiations of shading nets by analysing their energy exchange on them. The downward and upward solar and thermal radiation fluxes measured the energy balance below and above the net surface, respectively. Therefore, this study, addresses the data gap regarding the accurate determination of the thermal screen properties via a novel methodological approach to evaluate the screen energy-saving capacity for greenhouse energy efficiency. In addition, this study considered the permeability of screen materials. The model also simulated the real-life scenario considering all climatic conditions not considered in the previous studies, such as ambient pressure, external temperature, and wind speed.

Moreover, this study determines the effect of screen porosity on the overall heat transfer coefficient using the BES model by further investigating the thermal screen properties, including the thermophysical, radiometric, and aerodynamic properties based on their respective U-values. The accurate determination of the U-values for different thermal screens using BES would aid greenhouse energy system simulation and energy analysis and estimate the annual energy load in the greenhouse accurately, thereby limiting assumptions in predicting the energy loads for the energy-saving capacity of the greenhouse thermal screens. Moreover, information regarding the U-value and thermal performance would facilitate better production decisions by the screen-manufacturing industry.

## 2. Materials and methods

This research examines the thermophysical (thickness, density, thermal conductivity, and geometric features), radiometric (longwave, solar, and visible radiation), and aerodynamic (airflow and permeability) properties of the thermal screens, thus evaluating their overall heat transfer coefficients using TRNSYS and an experimental hotbox (U-value).

### 2.1. *Thermophysical property*

The thermophysical properties of 10 greenhouse screens were measured, as shown in Fig. 1. The thickness (mm) of the thermal screen was measured with an electronic digital calliper (TED PELLA, Inc., USA), and the thermal conductivity ($W\ m^{-1}\ K^{-1}$) was tested with a quick thermal meter (QTM-500, Kyoto Electronics MFG. Co., Ltd, Japan) (Rasheed et al., 2020).

The screens were classified as symmetrical or asymmetrical, opaque or transparent, with or without aluminum strips or layers (Balemans, 1989; Rafiq et al., 2019). As a result, the physical properties of the screen materials were used to categorise them as homogeneous or heterogeneous. Samples M1, M2, and M3 comprised of more than three distinct materials, as stated in Table 1, including an aluminised surface, non-woven polyester, casimiro cotton, and white polyester on the reverse surface. The Lawrence Berkeley National Laboratory (LBNL) software was used to feed these properties into TRNBuild, which generated a readable building file called DOE-2.

### 2.2. *Radiometric property*

To determine the thermal infrared and solar radiations through the selected materials, the radiometric features were examined using the radiation balance method. The radiometric properties were evaluated by calculating the radiation exchange between the thermal screen and the black fabric using the incoming and outgoing shortwave radiation (Rafiq et al., 2019), as well as the inward and outward longwave radiation (in $W\ m^{-2}$) from the sky (Rafiq et al., 2019; Blonquist et al., 2009; Rasheed et al., 2020). The radiation balance setup comprised of a 2 m by 2 m by 1 m (length × width × height) aluminum-steel frame. The radiometric experiment was conducted on the roof of the Agricultural Civil Engineering Department of Kyungpook National University in Daegu,

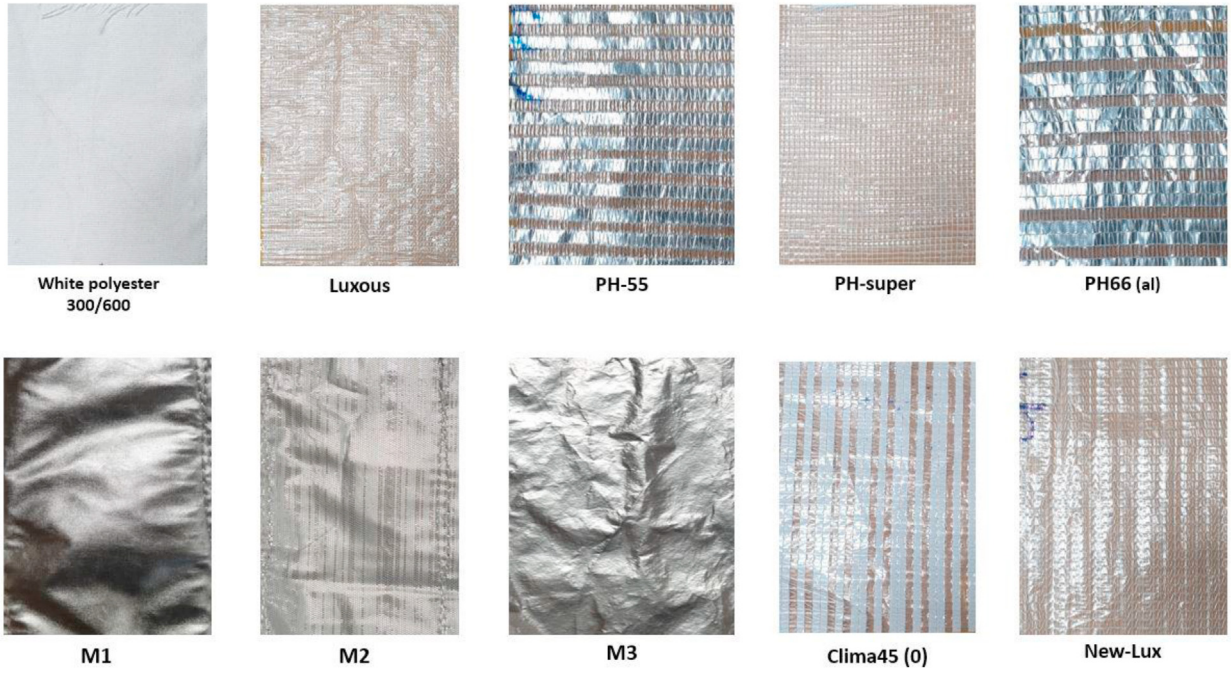


**Fig. 1 – Overview of the selected samples for the greenhouse energy-saving screen.**

**Table 1 – Material components of multilayered thermal screens.**

| SN | Name | Material Composition |
|---|---|---|
| 1 | M1 | Aluminum surface (Y1–Al/J1) + non-woven polyester + casimiro cotton + non- woven polyester + white polyester 300/300 |
| 2 | M2 | Aluminum strip surface (Y1–Al/DN1) + non-woven polyester + white polyester 300/300 |
| 3 | M3 | Aluminum surface (Y1–Al/W1) + non-woven polyester + casimiro cotton + non- woven polyester + white polyester 300/300 |

South Korea. The black fabric was stretched to cover the stand beneath the thermal screen at 0.5 m height to absorb the radiation passing through the thermal screen, while those were spread across the upper surface of the setup. As seen in Fig. 2, the black fabric reflected the radiation back to the thermal screen. The black cloth, covering the bottom of the frame, had known radiometric properties: emittance ($\varepsilon_b$) = 0.93, transmittance ($\tau_b$) = 0, and reflectance ($\rho_b$) = 0.07 (Rafiq et al., 2020).

Table 2 lists the radiometric sensors used in this study. These sensors were installed at the centre of the aluminum-steel frame, above the thermal screens, and between the thermal screens and the black fabric. As a result, the top sensors above the thermal screen recorded the sky radiation, while those between the thermal screen and the black fabric recorded radiation exchange between them. All necessary parameters were collected at 10-min intervals using two data

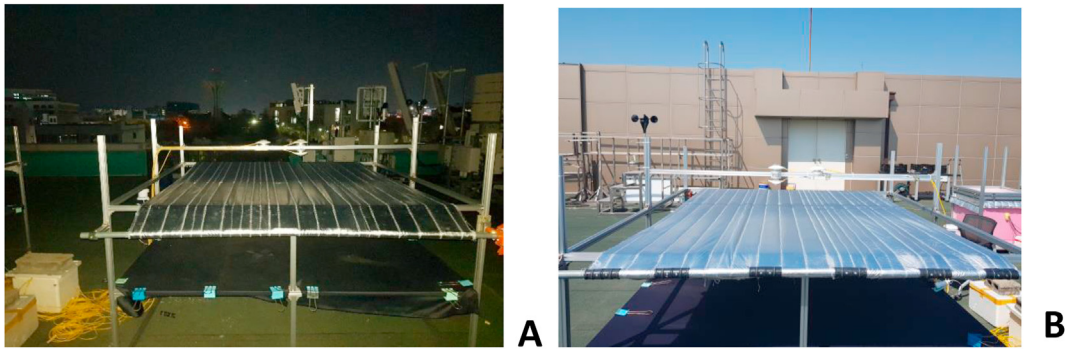


**Fig. 2 – Experimental setup for determining the radiometric property of the energy-saving screen during the (A) night time (B) daytime.**

**Table 2 – List of the sensors measuring the radiometric properties.**

| Parameter | Sensor | Unit | Data logger | Spectral range |
|---|---|---|---|---|
| Net longwave radiation | NR Lite2 Net radiometer (Kipp and Zonen, Netherlands) sensitivity 10 μV $W^{-1}$ $m^{-2}$, response time <20 s, W $m^{-2}$ sensor asymmetry <15% | LR-5042 (Kioki, Japan) | | 0.2–100 μm |
| Downward & Upward shortwave radiations | CPM3 pyranometer (Kipp and Zonen, Netherlands) sensitivity 11.54 μV $W^{-1}$ $m^{-2}$, response time <18 s, W $m^{-2}$ temperature sensitivity −10 to +40, tilt error <2%, zero offset <15 W $m^{-2}$. | LR-5042 (Kioki, Japan) | | 300–2800 nm |
| Downward longwave radiation | CGR3 pyrgeometer (Kipp and Zonen, Netherlands) sensitivity 14.54 μV $W^{-1}$ $m^{-2}$, response time <18 s, tilt W $m^{-2}$ error <2%, zero offset <5 W $m^{-2}$ | Model CR300 (Campbell scientific, Inc. USA) | | 4.5–42 μm |

recorders (loggers), as shown in Table 2. The materials were tested between 0600 and 1800 h, while the solar radiation was measured throughout the day. Conversely, longwave radiation was measured during the night from 1800 to 0600 h, the next day, as shown in Fig. 2. The radiometric properties of the thermal screens, i.e., the inward and outward directions of the longwave radiation were measured using net radiometers and pyrgeometers, as shown in Fig. 3. As a result, the pyranometer, which quantifies the solar radiation entering and leaving the screens, was used to measure the downward and upward shortwave radiations, as shown in Fig. 4.

The radiation balance equations were used to calculate the longwave radiation, as shown in Fig. 3. Thus, the longwave infrared radiation (W $m^{-2}$) determined the upward and downward radiations on the screen surface, where $Q_b$ is the upward longwave radiation from the thermal screens to the sky, and $Q_c$ is the upward longwave radiation from the thermal screens to the black fabric during the night (Abdel-Ghany et al., 2015).

$$Q_b = E_s + (\rho_L \times Q_a) + (Q_d \times \tau_L) \quad (1)$$

$$Q_c = E_s + (\tau_L \times Q_a) + (Q_d \times \rho_L) \quad (2)$$

where $Q_d$ is the inward longwave radiation from the black fabric toward the thermal screen (W m−2), $Q_a$ is the inward sky radiation toward the thermal screen, $\rho_L$ is the thermal screen's longwave reflectance, $\tau_L$ is the longwave transmittance of the thermal screen, $E_s$ is the emissive power of the thermal screen (W $m^{-2}$), a factor of the Stefan–Boltzmann's law.

$$Q_d = E_b + (\rho_b + \mu) \times E_s + (\rho_b - \mu) \times (\rho_L \times Q_d) + (\rho_b - \mu) \times (\tau_L \times Q_a) \quad (3)$$

$$\alpha_L = 1 - \rho_L - \tau_L \quad (4)$$

where $\alpha_L$ is the longwave absorptivity of the thermal screen (Al-Helal & Abdel-Ghany, 2011; Balocco et al., 2018; Hemming et al., 2017; Rafiq et al., 2021. Even though the number of equations equalled the number of unknowns, using the iteration method in MATLAB software to simultaneously solve Eqs. (1)–(3) resulted in Eq. (3), causing compatibility issues. To solve these equations simultaneously, micro (denoting $10^{-6}$) was subtracted from the reflected portions of $\tau_L \times Q_a$, and $\rho_L \times Q_d$, while added to the reflected portion of Es in Eq (3). The micro μ is the smallest assumed number that can tolerate the reflectance ($\rho_b$) of the black cloth with no effect on the radiation value and instead used as a tolerance to balance the iteration.

The shortwave radiation is expressed by the radiative property during the daytime (Fig. 4), measuring the inward and outward shortwave radiations on the screen materials, as specified in Eqs. (5) and (6).

$$S_b = (\rho_s \times S_a) + (\tau_s \times S_d) \quad (5)$$

$$S_c = (\rho_s \times S_d) + (\tau_s \times S_a) \quad (6)$$

where $S_b$ is the outward shortwave radiation from the thermal screen toward the sky, $S_c$ is the outward shortwave radiation from the thermal screen toward the black fabric, $\rho_s$ is the

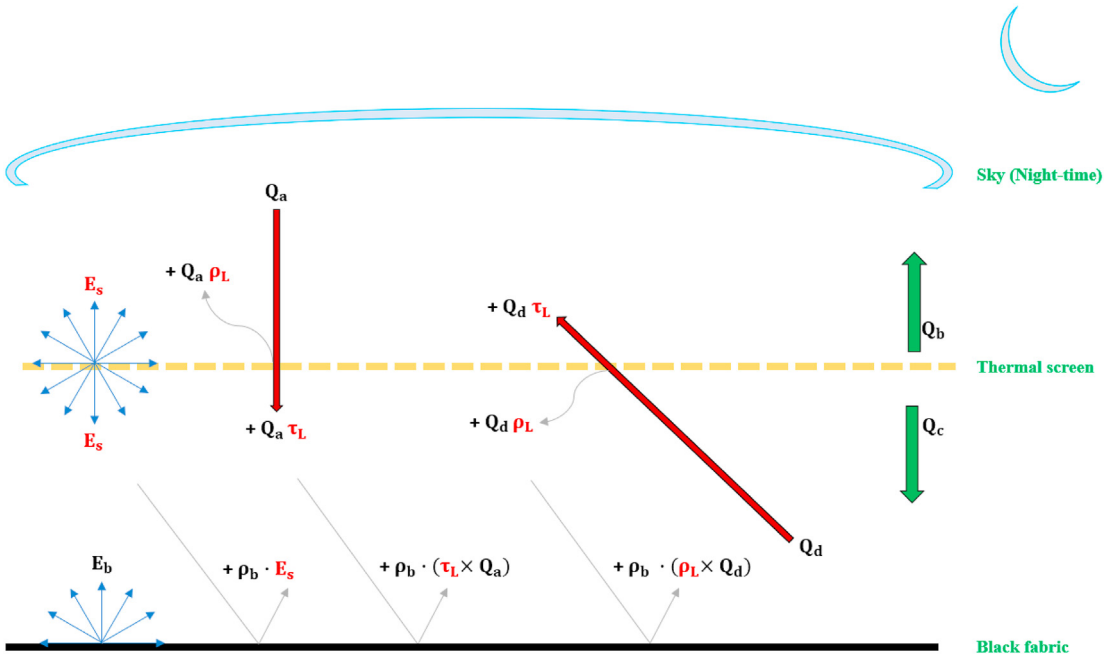


**Fig. 3 – Schematic diagram of the incoming ($Q_a$ and $Q_d$) and outgoing ($Q_b$ and $Q_c$) longwave radiations from the energy-saving screen during the night time.**

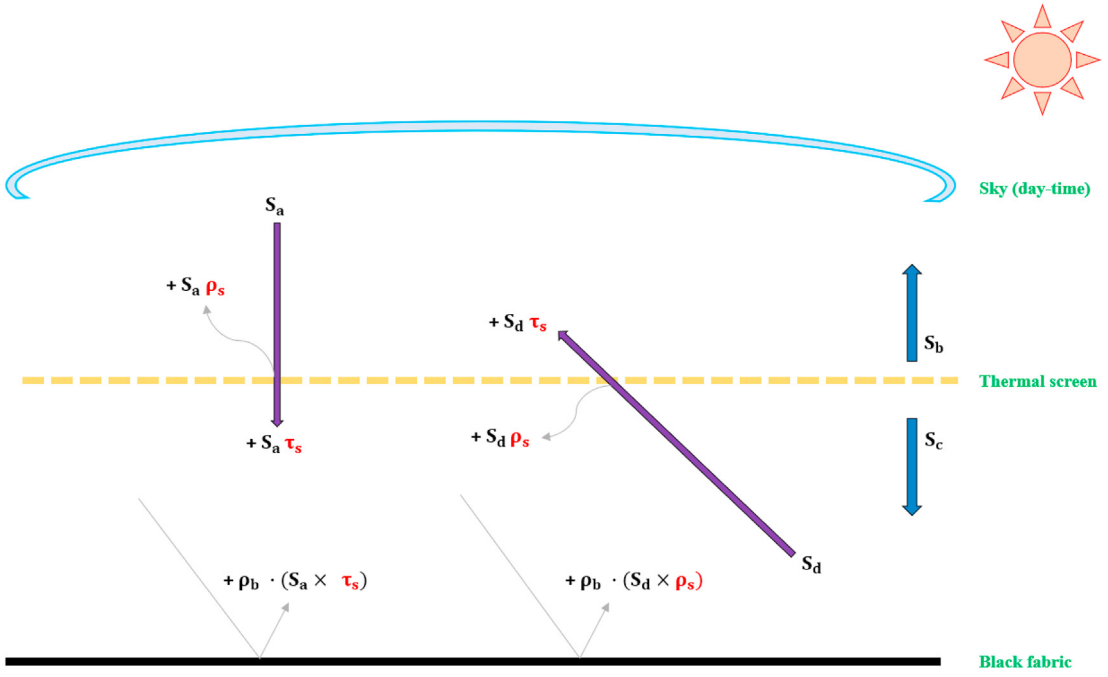


**Fig. 4 – Schematic diagram of the inward ($S_a$ and $S_d$) and outward ($S_b$ and $S_c$) shortwave radiations on the energy-saving screen during the daytime.**

reflectance of the thermal screen, $\tau_S$ is the transmittance of the thermal screen, and $S_a$ and $S_d$ are the sky downward shortwave radiation and radiation from the black fabric toward the thermal screen, respectively. Eqs. (1)–(4) were solved simultaneously by iteration (though the number of knowns equals the number of equations) using MATLAB (MATLAB 20B, MathWorks, USA) to determine the longwave radiation. Further, Eqs. (5) and (6) determined the shortwave radiation.

### 2.3. *Aerodynamic properties*

Air exchange occurs between the two sides of the screens via screen porosity. Air permeability accounts for heat and energy losses to the top compartment of the greenhouse (Hemming et al., 2017), thus used to determine the air exchange precisely. A laboratory-scale air-suction device with a draining water tank was developed to measure the air permeability of

the thermal screens, as shown in Fig. 5A. This apparatus operates on the air–water flow-suction mechanism, wherein gravity-induced air causes a pressure drop due to natural suction on the screen surfaces (Miguel, 1998). The closed system of the draining water tank mechanism was chosen because of its precise measurement of air permeability. The air-suction tank is a sealed container with three openings: two at the top (one for the screen holder, and the other for the water entry valve), and the third for water discharge, connecting to the flow sensor. The air-suction tank discharges water when valves D and C are open, as shown in Fig. 5B. The tank draws air from the surrounding environment into the system through the material pores, causing water to flow out. As a result, the volume of water released and its flow velocity leaving the system are identical to the air volume and airflow rate induced into the suction tank through the pores of the screens, respectively. The water flow rate is measured rather than the airflow rate through the material as water is easily quantifiable, thus making the measurement more accurate (Hemming et al., 2017). As shown in Fig. 5B, the thermal screen

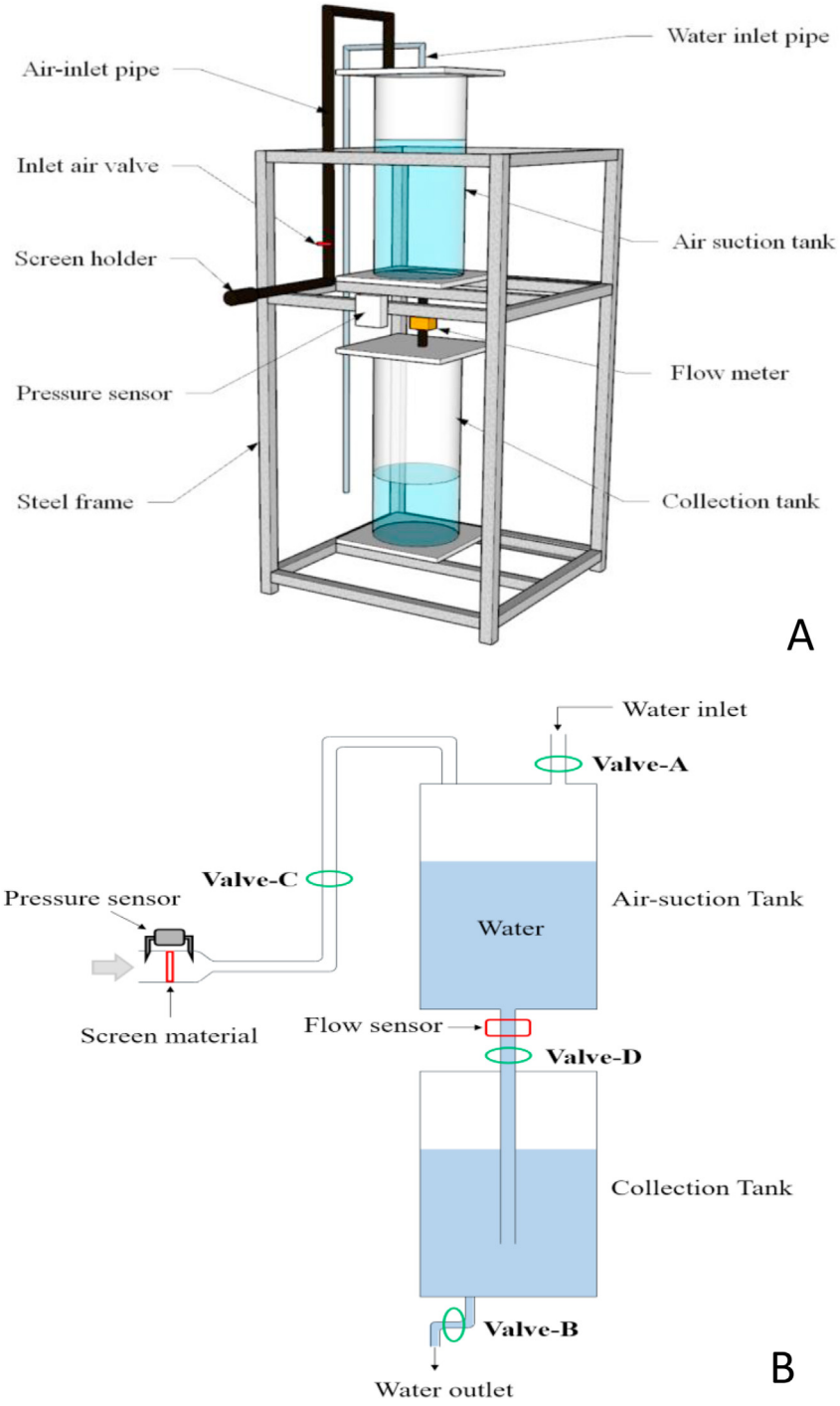


**Fig. 5 – (A) CAD design of the air-suction device (B) Schematic diagram of the air-suction device.**

was installed inside the screen holder, open to the ambient atmosphere, and connected to the upper part of the air-suction tank via a pipe. The sample screens were cut into 10 cm-diameter pieces and mounted on supporting rubber rings with inner and outer diameters of 8 and 10 cm, respectively. The volume of discharged water from the tank was measured with a flow sensor F-1000-RT with an operational range of 0–500 Pa (Blue-white industries, Ltd. USA), and the pressure drop of the screen was measured with a differential pressure transmitter DPUH-0500 with an operational range of 0–500 Pa (Sensys industries, Ltd. South Korea), which automatically recorded the pressure as air was sucked into the system. However, wind tunnel was not used to measure the screen permeability, as previously described (Hemming et al., 2017; Santolini et al., 2019).

Darcy's equation describes the fundamental interactions between air velocity and pressure difference when passing through two permeable materials. Darcy's law also describes an isothermal fluid moving at a slow and steady velocity through a material under a pressure gradient (Miguel, 1998). As a result, the Darcy equation holds for fluids moving at low speeds in laminar flow, and material permeability is determined by the material's ability to disperse fluids via pores (Hemming et al., 2017).

$$\frac{dP}{dx} = \frac{\mu_d}{K}\, u, \tag{7}$$

where $dP$ denotes the air pressure difference [Pa], $u$ is the air velocity [m s$^{-1}$], $K$ is the thermal screen permeability [m$^2$], $\mu_d$ is the dynamic viscosity of air [Pa s], and $x$ is the thickness of the thermal screen [m] (López-Martínez et al., 2020). In addition, the screen's infiltration rate was determined by the modified LBNL-model for estimating the rate of heat exchange by air infiltration in the greenhouse using the equivalent leakage area, flow coefficient, and a reference pressure difference as expressed in Eq. (8). The flow coefficient was determined by the material permeability and its aerodynamic properties.

$$Q_{frate} = K_t\, [\Delta P_r]^{0.66} \tag{8}$$

The airflow rate through the fabric is measured at a steady constant pressure of 50 Pa when effects of winds and buoyancy forces are eliminated (Jones et al., 2012). Furthermore, operational pressure differences are dynamic and typically an order of magnitude lower, at around 4 Pa or less for conversion to infiltration flowrate used to predict operational air leakage, according to (Balemans, 1989; Kraniotis, 2015). In building envelops, the average pressure across a leak is closer to 1 Pa than 50 Pa (Sherman & Chan, 2004). This study also concludes that a reference pressure of 1 – 4 Pa should be used to account for variations in natural pressure and to avoid high pressure, which can cause non-linear

**Table 3 – Properties of polystyrene.**

| Property | Value |
|---|---|
| Thickness (mm) | 100 |
| Density (kg m$^{-3}$) | 15 |
| Thermal conductivity (W m$^{-1}$ K$^{-1}$) | 0.033 |
| Specific heat capacity (kJ kg$^{-1}$ K$^{-1}$) | 1.25 |

**Table 4 – List of components and sensors used for the hotbox.**

| Components | Unit | Interval | Specifications | Data logger |
|---|---|---|---|---|
| PM-B540-W | watt | Hour | 200 V, 60 Hz, –10 °C–60 °C (AI power manager, South Korea) | |
| Wattmeter CM-100S | | | 600 W, 200 V, and 60 Hz (Comax Electric, China) | |
| Electric heater LTH-203 | | | 220V, 30A (South Korea) | |
| Heating control relay box | | | | Integrated type |
| HOBO MX2301A (Internal temperature & relative humidity) | °C<br>% | 10 min | Temperature<br>Range: - 40 °C-70 °C<br>Accuracy: ± 0.2 °C from –0 °C–70 °C<br>RH<br>Range: 0–100<br>Accuracy: ±2.5% from 10 to 100% (Onset, USA) | |
| HOBO TMCx-HD (External temperature) | °C | 10 min | Range: –40 °C–70 °C<br>Accuracy: ±0.25 °C from –40 °C–50 °C (Onset, USA) | HOBO 4-Channel Analogue Data Logger UX120-006M (Onset, USA) |
| Thermocouple probes (Internal and external surface temperature) | °C | 10 min | Range: –270 °C–1260 °C<br>Accuracy: ±0.25 °C from –40 °C to 50 °C | HOBO 4-Channel Thermocouple Data Logger UX120-014M (Onset, USA) |
| RS3-B (Solar radiation shield) | | | Range: –40 °C–75 °C<br>Weight: 113 g (Onset, USA) | |

**Table 5 – Thermophysical properties of the thermal screens.**

| SN | Sample (trade name) | Thickness (mm) | Thermal conductivity ($Wm^{-1}$ $K^{-1}$) | Layer | Symmetric/ Asymmetric | Al-strip | Composition |
|---|---|---|---|---|---|---|---|
| 1 | White Polyester 300/600 | 0.34 | 0.1066 | Single | Symmetric | Non | homogenous |
| 2 | Luxous | 0.31 | 0.0558 | Single | Symmetric | Non | homogenous |
| 3 | PH-55 | 0.41 | 0.1486 | Single | Asymmetric | ½ | homogenous |
| 4 | PH-super | 0.33 | 0.0946 | Single | Symmetric | Non | homogenous |
| 5 | PH-66al | 0.46 | 0.1573 | Single | Asymmetric | 2/3 | homogenous |
| 6 | M1 | 1.74 | 0.0440 | Multi | Asymmetric | Non | heterogenous |
| 7 | M2 | 0.9 | 0.6623 | Multi | Asymmetric | Non | heterogenous |
| 8 | M3 | 1.85 | 0.0486 | Multi | Asymmetric | Non | heterogenous |
| 9 | Clima45 (0) | 0.24 | 0.0660 | Single | Symmetric | Non | homogenous |
| 10 | New-lux | 0.25 | 0.0525 | Single | Symmetric | Non | homogenous |

**Table 6 – Radiometric properties of the thermal screens.**

| SN | Sample (Trade Name) | Surface | Thermal Radiation (2500 –40,000 nm) | | | Solar Radiation (300–2500 nm) | |
|---|---|---|---|---|---|---|---|
| | | | ε | ρ | τ | τ | ρ |
| 1 | White Polyester 300/600 | Front | 0.94 | 0.04 | 0.02 | | |
| | | Back | 0.94 | 0.04 | 0.02 | | |
| 2 | Luxous | Front | 0.44 | 0.18 | 0.38 | 0.58 | 0.30 |
| | | Back | 0.44 | 0.18 | 0.38 | 0.57 | 0.25 |
| 3 | PH-55 | Bright | 0.25 | 0.35 | 0.40 | 0.38 | 0.43 |
| | | Dull | 0.31 | 0.36 | 0.33 | 0.41 | 0.31 |
| 4 | PH-super | Front | 0.60 | 0.02 | 0.38 | | |
| | | Back | 0.60 | 0.02 | 0.38 | | |
| 5 | PH-66al | Bright | 0.32 | 0.58 | 0.10 | 0.17 | 0.67 |
| | | Dull | 0.52 | 0.38 | 0.10 | 0.17 | 0.57 |
| 6 | M1 | Front | 0.01 | 0.99 | <0.01 | <0.01 | 0.99 |
| | | Back | 0.51 | 0.49 | <0.01 | <0.01 | 0.49 |
| 7 | M2 | Front | 0.02 | 0.98 | <0.01 | <0.01 | 0.98 |
| | | Back | 0.51 | 0.49 | <0.01 | <0.01 | 0.49 |
| 8 | M3 | Front | 0.01 | 0.99 | <0.01 | <0.01 | 0.99 |
| | | Back | 0.51 | 0.49 | <0.01 | <0.01 | 0.49 |
| 9 | Clima45 (0) | Front | 0.48 | 0.17 | 0.35 | 0.38 | 0.50 |
| | | Back | 0.55 | 0.14 | 0.31 | 0.38 | 0.48 |
| 10 | New-lux | Front | 0.45 | 0.30 | 0.26 | 0.58 | 0.30 |
| | | Back | 0.42 | 0.27 | 0.31 | 0.57 | 0.25 |

**Table 7 – Aerodynamic properties of the thermal screen materials.**

| SN | Sample (trade name) | Permeability ($m^2$) | Infiltration flow rate per unit area ($cm^3$ $cm^{-2}$ $s^{-1}$) | Hotbox air change per hour ACH ($h^{-1}$) |
|---|---|---|---|---|
| 1 | White Polyester 300/600 | $6.51E^{-12} \pm 8.9E^{-13}$ | 0.086 | 5.1 |
| 2 | Luxous | $1.71E^{-11} \pm 1.0E^{-12}$ | 0.179 | 10.8 |
| 3 | PH-55 (open) | $7.25E^{-10} \pm 4.0E^{-11}$ | 2.344 | 140.6 |
| 4 | PH-super | $2.53E^{-11} \pm 3.0E^{-13}$ | 0.220 | 13.2 |
| 5 | PH-66al | $3.41E^{-11} \pm 2.7E^{-12}$ | 0.182 | 10.9 |
| 6 | M1 | $2.66E^{-13} \pm 2.2E^{-14}$ | 0.002 | 0.1 |
| 7 | M2 | $1.42E^{-12} \pm 2.4E^{-14}$ | 0.028 | 1.7 |
| 8 | M3 | 0.00 | 0.00 | 0.0 |
| 9 | Clima45 (0) | $1.49E^{-11} \pm 1.3E^{-12}$ | 0.151 | 9.1 |
| 10 | New-lux | $1.33E^{-11} \pm 1.6E^{-13}$ | 0.194 | 11.7 |

effects that do not accurately represent the actual pressure (Sherman & Chan, 2004). Hemming et al. (2017) use an experimental greenhouse to measure air velocity through the screens pore in order to characterise the air permeability values of various screens. Therefore, a range of air velocities lower than 0.2 m $s^{-1}$ was recorded and the maximum air speed of 0.2 m $s^{-1}$ is necessary to accurately characterise the aerodynamic properties. This present study used a reference pressure of 1Pa as an estimated pressure difference based on López et al. (2016)'s pressure drop–velocity relationship model for greenhouse screens, and air velocity of 0.2 m $s^{-1}$ through the screens (Hemming et al., 2017).

### 2.4. BES model

TRNSYS is a BES software used to create the geometry of the hotbox model. Firstly, the 3D model of the Hotbox was created using Transys3d, a Google SketchUpTM extension (add-in). Second, the model was imported into TRNBuild as an IDF file to define the hotbox material properties. Polystyrene properties, thermal screens, and outside weather parameters were used as the input parameters. The walls of the hotbox were composed of polystyrene insulation, and the wall properties were chosen from the TRNBuild library, as shown in Table 3. Third, the thermal screen properties included longwave radiation, shortwave radiation, physical properties, and aerodynamic properties, as shown in Tables 5–7, processed using the Lawrence Berkeley National Laboratory (LBNL) Window 7.4 software, as shown in Tables 5–7. Finally, as shown in Fig. 7, the DOE-2 data file was generated and imported into TRNBuild.

The TRNSYS studio consisted of the following components, called "type" for the hotbox simulation: a multi-zone building (type56), weather data reader (type9c), solar radiation processor (type16a), printer (type25c), plotter (type65c), and an equation editor, as shown in Fig. 8. The hourly outside weather information, including the ambient air temperature, sky temperature, wind speed, and ambient pressure was collected from the Korean Metrological Administration (KMA). The weather reader processed the data to simulate the actual external climatic conditions. All these components were interconnected and linked to type56 as inputs and outputs. The TRNBuild generated the building information stored as a b18-file, defining all the hotbox input parameters. Also, the plotter and printer displayed the outputs from the simulation. The model determined the heat flux through the thermal screens while considering them as permeable or impermeable. Permeability is a measure of airflow rate through the pore of screen materials, accounting for leakages or losses.

According to TRNSYS 18, TRNBuild allows a standard infiltration simulation by setting the screen material airflow rate in terms of air change per hour (ACH) $h^{-1}$ as a constant value or input variable. However, the airflow rate is operated with a Boolean controller (ON/OFF), switched ON considering the infiltration and OFF otherwise. Therefore, the ACH ($h^{-1}$) expressed below, is in accordance with the ASHRAE standard:

$$ACH = \frac{A_s \times Q_{frate}}{V_{box}} \tag{9}$$

where $A_s$ is the hotbox surface area covered with the screen ($m^2$), $V_{box}$ is the volume of the hotbox ($m^3$), and $Q_{frate}$ is the airflow rate of the screen area ($m^3\ m^{-2}\ h^{-1}$).

The hotbox geometry's overall heat loss and the model's heat transfer were used (Solar Energy Laboratory, 2018, pp. 7–36), as depicted below:

$$Q_{loss} = Q_{conv} + Q_{rad} + Q_{inf} \tag{10}$$

The convective heat loss from the hotbox represented the loss between the hotbox surface and the external environment, as shown below:

$$Q_{conv} = H_e\ (T_{es} - T_a) \tag{11}$$

The model used the sky temperature equation to determine the external surface longwave radiation exchange and the radiative heat transfer, as stated in Eq. (12) (Asdrubali et al., 2019; SCL, 2018, pp. 7–36; Zhang et al., 2017):

$$Q_{rad} = \sigma\ \varepsilon_0\ \left(T_{es}^4 - T_{fsky}^4\right) \tag{12}$$

$$T_{fsky} = \left(1 - f_{s,sky}\right).\ T_{grd} - f_{s,sky}\ .\ T_{sky} \tag{13}$$

$$T_{sky} = T_a(\varepsilon_0 + 0.8\ (1\ -\ \varepsilon_0)C_{cover})^{0.25} \tag{14}$$

Also, the infiltration heat loss due to airflow through material pore from the hotbox was described by the following equation:

$$Q_{inf} = V\ \rho\ C_p(T_i - T_a) \tag{15}$$

The total heating demand equals the heat loss from all the hotbox surfaces, calculated individually for each surface by the model. As a result, the heat loss through the screen was used to calculate the materials' U-value.

### 2.5. Hotbox model validation

A statistical analysis of the coefficients of determination $R^2$ was performed to evaluate the hotbox model's performance, quantitatively expressing the model's performance, as shown in Eq (16). As a result, the $R^2$ accuracy value ranged from 0 to 1, with a value closer to 1 indicating that the model is accurately fit. As a result, the results were statistically analysed using the Microsoft Excel 2016 statistical package (Ogunlowo et al., 2021). The model's fitness was validated by comparing white polyester's simulated and experimental U-values. A t-test statistical analysis was also performed to compare the computed U-value (both permeable and impermeable cases) of each material averaged over different trials and experimental U-value to determine the significance of difference in the results. The study was conducted at a 5% level of significance.

$$R^2 = 1 - \left[\frac{\sum_{i=0}^{n}\left(U_i^{exp} - U_i^{sim}\right)^2}{\sum_{i=0}^{n}\left(U_i^{exp} - U_{avg}^{exp}\right)^2}\right] \tag{16}$$

### 2.6. Experimental hotbox

Four calibrated laboratory hotbox devices were constructed in accordance with ASTM standards C 236–89 and C 976 to investigate the overall heat transfer coefficients (U-values) of greenhouse thermal screens. These devices were made from polystyrene insulation material and an aluminum frame for external support and rigidity. The boxes are of two sets which were 800 × 800 × 800 mm and 700 × 700 × 700 mm (*length, width, and height*) in volumetric dimensions, respectively, with the wall thickness of 100 mm (Fig. 6). The Hotbox had an opening at the top, called the window, accommodating the screen materials under investigation. The box chamber was split in 700 and 600 mm heights to enable the testing of screen samples. To prevent air leakage from the system, a section of polystyrene was placed on the screen sample and metal

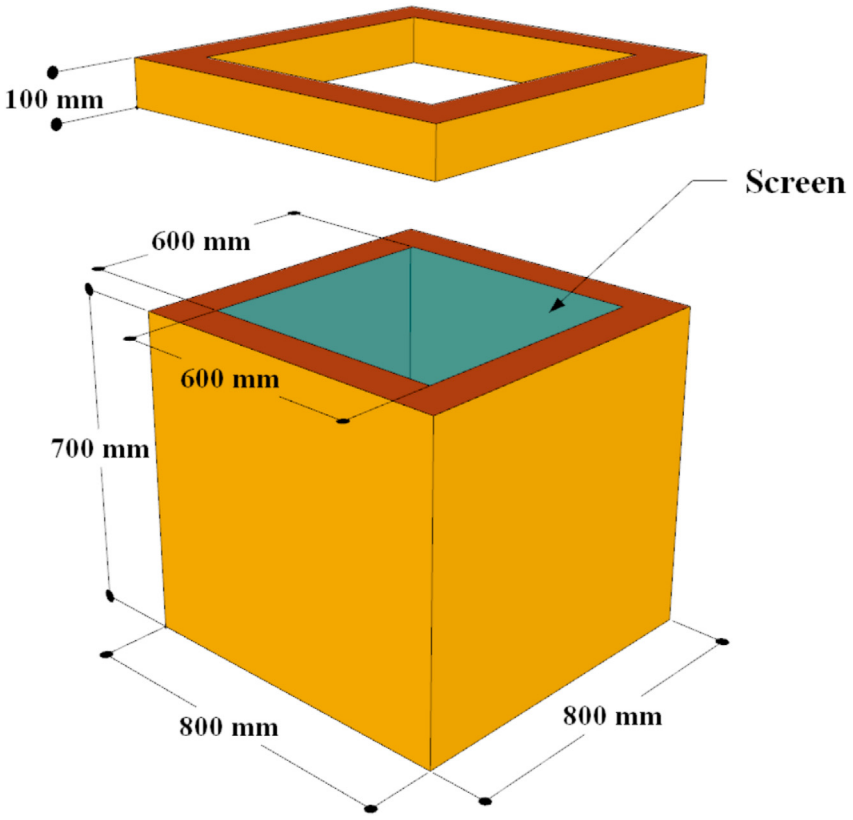


**Fig. 6 – Trnsys3d sketch of the hotbox simulated model.**

frame, held to the body frame by a belt rope. A sponge-corner cushion, bonded to the upper face of the polystyrene and lower surface of the polystyrene cover to enable airtight window access and a smooth surface match, prevented leakages between the upper hotbox surface and the screen sample.

The hotbox heating system operated at a preset temperature of 40 °C to maintain the required inner chamber temperature using an electric heater. The heating source was strategically placed at the centre of the specimen box for uniform heat distribution during the experiment (Fig. 9), and the hotbox components are listed in Table 4. Two external HOBO TMCx-HD sensors measured the ambient temperature accurately with a solar radiation shield (RS3-B), preventing the climatic influence on the sensor measurement. These sensors were connected to a 4-channel analog data logger obtaining

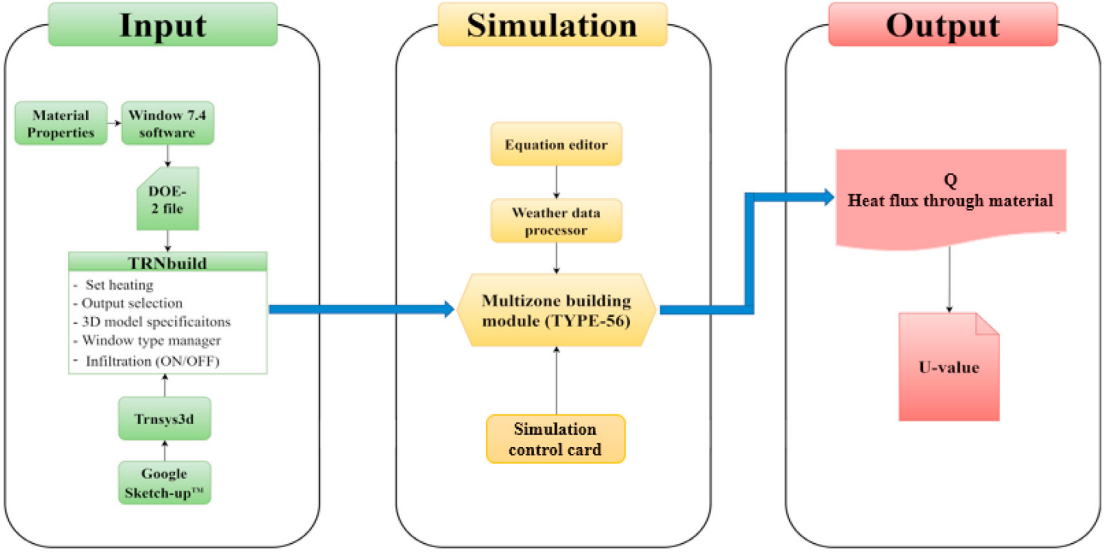


**Fig. 7 – Flowchart diagram of the hotbox TRNSYS model.**

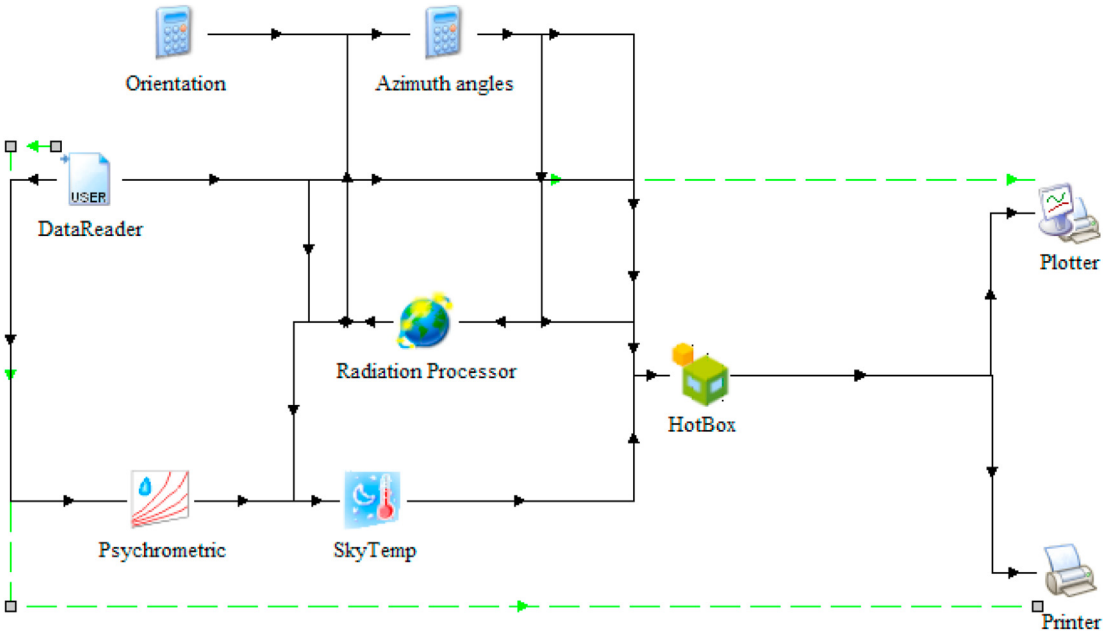


**Fig. 8 – TRNSYS Simulation studio hotbox model.**

the readings at 10 min intervals. The internal air temperature was automatically measured and recorded by two HOBO MX2301A sensors. The internal and external surface temperatures were measured by four thermocouple probes connected to a HOBO UX120-06M data logger, recording the readings at 10 min intervals. The power input of the electric heater was measured by a Wattmeter (Watts), and a heating control box regulated the air temperature inside. Additionally, a control box was positioned at the outer surface of the hotbox, connected to the thermocouple measuring the air temperature in the hotbox and the electric heater regulating the hotbox temperature. The experiment was conducted during the winter night time, suitable for the thermal screen usage. The optimum ambient climatic conditions were between 2100 and 0500 h, as shown in Fig. 10. However, this hotbox method did not consider the humidity transportation previously considered by (Feuilloley & Issanchou, 1996; Geoola et al., 2009).

These experiments were conducted at night to observe the heat loss during the night time. However, if the hotbox walls and bottom are considered adiabatic with stable heat transfer through the thermal screens, and the system is in a steady state, then the experimental process is considered to follow the thermal equilibrium theory, stated in Eq. (17):

$$U = \frac{Q}{A(T_i - T_a)} \tag{17}$$

where U is the overall heat transfer coefficient (W $m^{-2}$ $K^{-1}$), Q

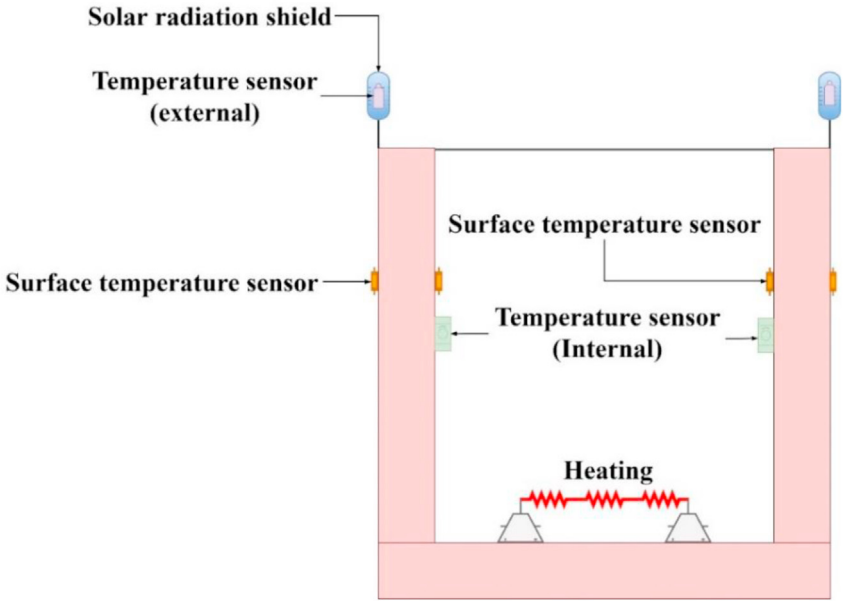


**Fig. 9 – Schematic diagram of the hotbox.**

is the heat loss through the thermal screen (watts), A is the cross-sectional area of the test sample ($m^2$), $T_i$ is the inner air temperature (°C), and $T_a$ is the ambient temperature (°C). However, Eq. (17) did not consider energy loss through the hotbox walls, which must be estimated as the system was not adiabatic. Thus, the hotbox wall surface temperatures for both the internal and external surfaces were measured to quantify the energy loss through the walls. The box's energy balance equation is as follows:

$$Q = Q_r - Q_w \tag{18}$$

where, $Q_r$ is the heater's heating power (watt) and $Q_w$ is the heat loss through the hotbox surfaces: sidewalls and floor, (watt).

$$Q_w = \frac{\lambda\, S_w\, (T_{is} - T_{es})}{L} \tag{19}$$

where $S_w$ is the surface area ($m^2$), λ is the thermal conductivity of the polystyrene insulation ($W.m^{-1}.K^{-1}$), $T_{is}$ is the internal surface temperature (°C) $T_{es}$ is the external surface temperature (°C), and L is the thickness of the Hotbox (m).

## 3. Results and discussion

### 3.1. Thermophysical property

The thermal screens are classified as symmetric or asymmetric, based on their thermophysical properties. The surface (identical or unidentical) of the screen material influenced the classification, as indicated in Table 5. The symmetric displays exhibited same chemical composition and face colour on both sides, while those of the asymmetric displays varied, making the sides dull or bright, thus resulting in different physical attributes. Greenhouse thermal screens can also be divided into homogeneous and heterogeneous, and the physical attributes of the screen materials substantially impacted their thermal qualities. In this study, PH-super material showed an experimental thermal conductivity of 0.094 W $m^{-1}$ $K^{-1}$, similar to 0.08 W $m^{-1}$ $K^{-1}$ reported by (Rasheed et al. 2020). The samples M1, M2, and M3 showed identical physical properties: asymmetric, aluminised surface, and multilayer screens; however, the material compositions and thicknesses differed, as indicated in Table 5. M1, M2, and M3 showed the thermal conductivities of 0.0440 (lowest), 0.6623 (highest), and 0.0486 W $m^{-1}$ $K^{-1}$ and thicknesses of 1.74, 0.9, and 1.85 mm (highest), respectively. These results demonstrated the effect of screen thickness on thermal resistance rather than thermal conductivity (Hung Anh & Pásztory, 2021).

As indicated in Table 1, these heterogeneous screens comprised of over three different materials: an aluminised surface, non-woven polyester, casimiro cotton, and white polyester on the rear surface, thus commonly used as thermal screens in greenhouses to decrease heat loss. Luxous, PH-super, New-Lux, and Clima45 (0) are symmetric single-layer film strips and transparent materials (Rafiq et al., 2019). However, PH-55 and PH-66al are asymmetric (homogenous) materials, which is a combination of aluminum strips and open shading with minimum airflow resistance, showing minor surface composition differences. PH-55 and PH-66al materials show a high thermal conductivity when compared to different single-layer screens due to the quick heat transfer by the glossy aluminum stripes.

### 3.2. Radiometric property

Table 6 shows the radiometric characteristics of the thermal screens, including the longwave radiation (transmissivity, reflectivity, and emissivity) and solar radiation. The opaque and aluminised front surfaces of the thermal screens M1, M2, and M3 imparted high longwave reflectance (above 95%) and low transmittance (below 1%). Conversely, the reverse surfaces exhibited estimated reflectance and emittance of 49% and 51%, respectively. Varied material compositions of the front and rear surfaces induced asymmetry in the screens, resulting in different incoming and outgoing radiometric characteristics. PH-55 and PH-66al demonstrated a higher reflectance on the front (bright) surface than the back (dull) surface. The contrast of shiny aluminum film strips on the front face with the dull aluminum strips on the back surface resulted in a variation in their reflectance levels. PH-super, Luxous, New-Lux, and Clima45 (0) showed high transmittance and diffusion and low reflectance values on both sides owing to their symmetry (transparency) with equal radiations on both sides. For example, Luxous (LD-13) showed the reflectance, transmittance, and emittance of 0.158, 0.382, and 0.46, respectively, according to (Rafiq et al. 2019). These results are fairly consistent with the Luxous data showing the reflectance, transmittance, and emittance values of 0.18, 0.38, and 0.44, respectively.

The homogeneous materials PH-55, PH-66al, and Clima45 (0) are asymmetric because the surface has a, which influences the observed radiation property. White polyester showed the maximum emittance (longwave radiation) of 94% as compared to other materials, but low reflectance and transmittance of 4% and 2%, respectively. In conclusion, a thermal screen material's physical properties and chemical composition have a significant impact on its radiation property.

### 3.3. Aerodynamic properties

The aerodynamic properties of different samples, including the permeability and airflow rate per unit area are depicted in Table 7. Luxous showed a permeability value of 1.71 $E^{-11}$ $m^2$, slightly lower than the 1.93 $E^{-11}$ $m^2$ reported by Hemming et al. (2017). The aerodynamic properties of porous screens are heavily influenced by its material porosity. PH-55 showed the highest permeability due to its high porosity and infiltration rate per unit area of 2.34 $cm^3$ $cm^{-2}$ $s^{-1}$, less than the maximum air flux exchange of 2.5 $cm^3$ $cm^{-2}$ $s^{-1}$ reported by (Miguel, 1998). This screen also contained an open strip for an unrestricted airflow through the material. However, the experiment proved that M3 was impervious to air, thus showed no airflows, indicating that the sample material showed zero permeability, thus preventing any air passage through the pores. In addition, M1 and M2 showed low permeabilities, limiting the air passage through the pores.

**Fig. 10 – Experimental hotbox device.**

### 3.4. *Model simulation and validation*

The overall heat transfer coefficients of various thermal screens were calculated using the model. The $R^2$-values of the simulated (considering material permeability and impermeability) and experimental U-values for white polyester were 0.87 and 0.88, respectively (Fig. 11), demonstrating the reasonable accuracy of the model in predicting the U-value of the thermal screen.

Similarly, the percentage error in the U-values of white polyester computed as impermeable and permeable were 32.4% and 2.4%, respectively, as shown in Table 8. Thus, while the impermeable screen showed a significant inaccuracy in results, the uncertainty was reduced for the permeable screen, yielding more accurate results. These indicated a decent match for the model and a fair agreement with the experiment U-values.

Without considering the material permeability, a study found the U-value of white polyester 300/600 as 5.5 W $m^{-2}$ $K^{-1}$ (Rasheed et al. 2018a), and the computed impermeable result showed a comparable U-value of 5.5 W $m^{-2}$ $K^{-1}$. A previous research study, the actual and estimated U-values for polyethylene covering screens were 9.2 and 11.37 W $m^{-2}$ $K^{-1}$, respectively (Vitoshkin et al., 2021). Also, Feuilloley and Issanchou (1996) reported the experimental and simulated U-values of 9.2 and 10.5 W $m^{-2}$ $K^{-1}$, respectively, for a multilayered (LDPE + mineral dope) polyethylene. Although it is difficult to compare the results of these reported studies due to the diverse methods and materials used, the reported findings depicted in Fig. 11 indeed exhibit some parallels with our findings. A comparable experimental hotbox was employed to investigate the U-value of the covering screen, following the same pattern as our study. Another study found that a single-layered polyethylene had a U-value of 9.7 W $m^{-2}$ $K^{-1}$ (Geoola et al., 2009). (Diop et al. 2012) also found that single- and double-layered polyethylene showed large U-values of 7.7 and 10.4 W $m^{-2}$ $K^{-1}$, respectively.

The U-values of different materials were explored after the model was successfully validated, and the influence of screen permeability was observed for the same. As a result, a t-test statistical analysis was conducted to examine the significant difference between the average U-value of different trials for both computed permeable and impermeable cases against the experimental outcomes.

Furthermore, the t-test demonstrated a significant difference between the computed impermeable U-value and the experimental U-value for White polyester, Luxous, PH-55, PH-super, Ph-66, Clima45 (0), and New-Lux. In contrast, at a 5% threshold of significance, M1, M2, and M3 showed no significant difference. Thus, the multilayered thermal screens M1, M2, and M3 were practically airtight with minimal heat loss through the pores and remained unaffected by the wind speeds of 5 m $s^{-1}$, as illustrated in Fig. 11. Also, wind speed of less than 2.5 m $s^{-1}$ affected the U-value of other screens at a range of ±0.5 W $m^{-2}$ $K^{-1}$. Additionally, only PH-55 revealed a significant difference when comparing the computed permeability U-value to the experimental U-value at a 95% confidence level. However, the other thermal screens showed similar U-values, reflecting that the permeability of materials should be considered when using thermal screens to save energy in greenhouses.

### 3.5. *Overall heat loss coefficient*

The U-value of thermal screens for the experimental hotbox and simulation are discussed in this section, as shown in Table 8. According to the experimental U-value data, Sample M1 showed the lowest U-value of 3.9 W $m^{-2}$ $K^{-1}$, while those of white polyester, Luxous, PH-55, PH-super, PH-66, M2, M3, Clima45 (0), and New-Lux were 110%, 144%, 897%, 177%, 133%, 49%, 18%, 123%, and 151% higher than M1, respectively. The simulation U-value (computed impermeable) results revealed that Luxous had the lowest U-value of 3.8 W $m^{-2}$ $K^{-1}$, and those for white polyester, PH-55, PH-super, PH-66, M1, M2, M3,

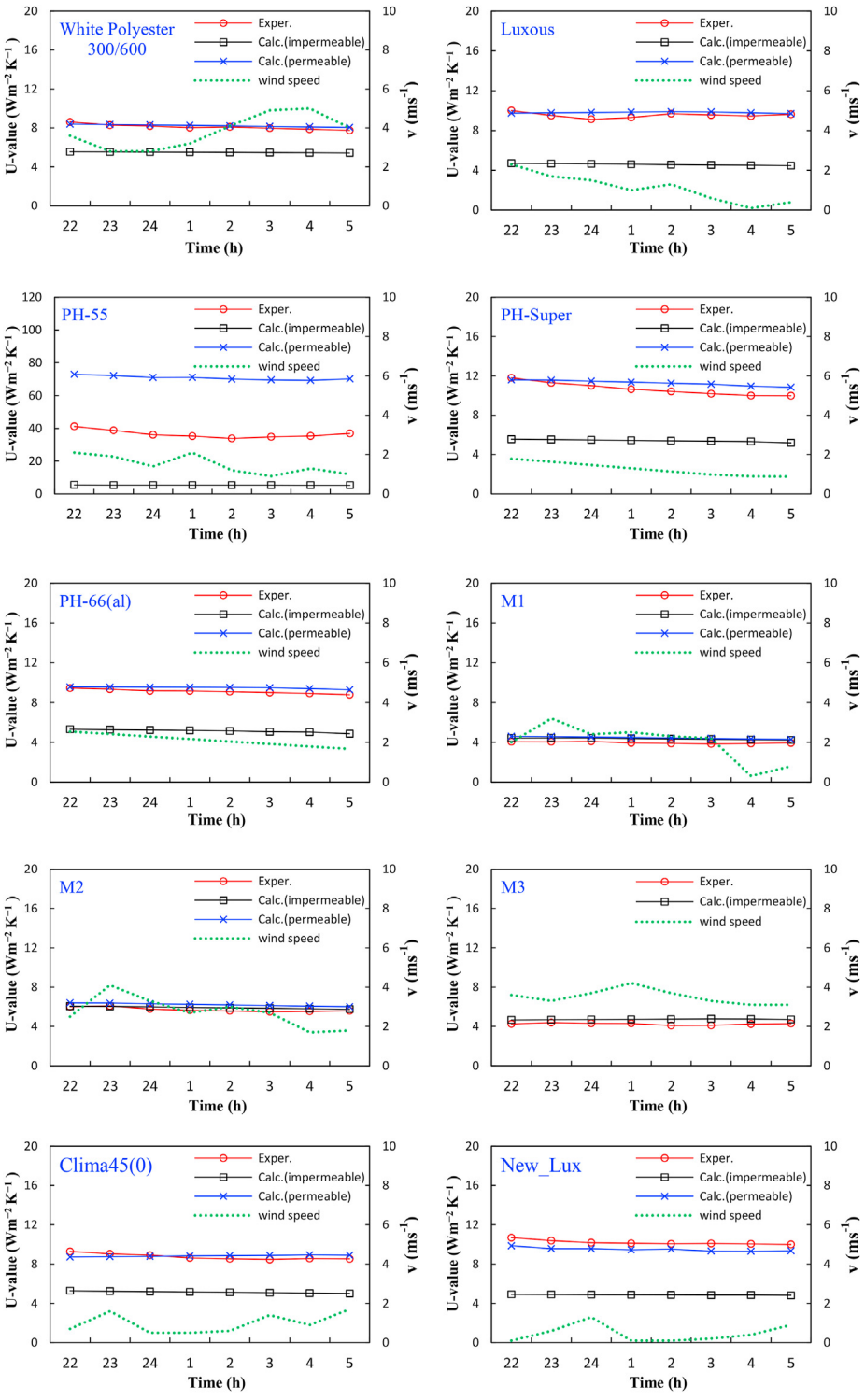


**Fig. 11 – Simulation and experimental U-values of different energy-saving screens with the wind speeds.**

Clima45 (0), and New-Lux were 45%, 16%, 37%, 21%, 13%, 42%, 16%, 18%, and 5%, higher than Luxous, respectively. Also, the simulated U-value (for computed permeable) results for samples M1 and M3 were the lowest at 4.4 W $m^{-2}$ $K^{-1}$, and white polyester, Luxous, PH-super, PH-66, M2, Clima45 (0), and New-Lux, showed the values of 82%, 105%, 161%, 123%, 41%, 102%, and 118%, higher than M1 and M3, respectively. Nonetheless, there was no significant difference in the U-values of samples M1, M2, and M3 for both experimental and simulated results. The material had a high resistance to air movement, lowering the heat loss caused by screen infiltration.

Sample M3 was also completely impermeable, preventing any heat escape through the pore. Conversely, PH-55

**Table 8 – Comparison of the computed and experimental values of the overall heat loss coefficients of the thermal screens.**

| SN | Sample (trade name) | Computed U-value (W $m^{-2}$ $K^{-1}$) | | Experimental U-value (W $m^{-2}$ $K^{-1}$) |
|---|---|---|---|---|
| | | Impermeable | Permeable | |
| 1 | White polyester 300/600 | 5.5 | 8.0 | 8.2 |
| 2 | Luxous | 3.8 | 9.0 | 9.5 |
| 3 | PH-55 (open) | 4.4 | 72.1 | 38.9 |
| 4 | PH-super | 5.2 | 11.5 | 10.8 |
| 5 | PH-66 (al) | 4.6 | 9.8 | 9.1 |
| 6 | M1 | 4.3 | 4.4 | 3.9 |
| 7 | M2 | 5.4 | 6.2 | 5.8 |
| 8 | M3 | 4.4 | 4.4 | 4.6 |
| 9 | Clima45 (0) | 4.5 | 8.9 | 8.7 |
| 10 | New-lux | 4.0 | 9.6 | 9.8 |

contained a broad open strip accounting for around 45% of the overall material size. These large holes allowed unfettered airflow with little resistance to airflow and other climatic elements to have a considerable impact on heat loss. Because of little air resistance, the pressure difference between the PH-55 surfaces tended to zero (0 Pa), affecting its infiltration rate and the U-value. 1 Pa as the reference pressure difference altered the infiltration rate, thereby affecting the U-value. For example, the simulated U-value will be reduced if half the pressure difference (i.e., 0.5 Pa) was used, similar to the experimental U-value. As a result, PH-55 is a greenhouse open-shading screen typically used in conjunction with other single thermal screens to improve the thermal performance and reduce the humidity to provide a conducive environment for plant development (Baeza et al., 2020).

The computed and experimental U-value results for samples M1, M2, and M3 were fairly consistent. These samples retained more heat and were impervious to water and air movements. This research concludes that materials with high thickness, low permeability, low IR emissivity, and high IR reflectance have the lowest U-value and are more suited for greenhouse heat retention based on a combination of the properties of the analysed sample.

## 4. Conclusions

The TRNSYS model and an experimental hotbox were used to investigate the attributes of commercial greenhouse thermal screens and calculate the overall heat transfer coefficient to assess the thermal performances (U-values) of the screens. To quantify the properties of the screens, an experimental methodological approach was adopted, later used in BES to obtain the U-values of the screens. A practical hotbox method was also proposed to validate the simulated model. When evaluating the screen materials for energy-saving purposes, this method can improve the efficacy of the thermal screen in greenhouse energy simulation and pre-design procedures.

The screens M1 and M3 exhibited the lowest computed permeable U-values of 4.4 W $m^{-2}$ $K^{-1}$, while white polyester, Luxous, PH-super, PH-66, M2, Clima45 (0), and New-Lux showed 82%, 105%, 161%, 123%, 41%, 102%, and 118% higher values than M1 and M3. M1 showed a U-value of 3.9 W $m^{-2}$ $K^{-1}$, while white polyester, Luxous, PH-55, PH-super, PH-66, M2, M3, Clima45 (0), and New-Lux showed 110%, 144%, 897%, 177%, 133%, 49%, 18%, 123%, and 151% higher values, respectively, according to the experiment. The t-test analysis of U-value data from the simulation and experimental hotbox demonstrated the most significant results for M1, M2, and M3, with no significant differences among other screens.

The influence of material permeability on the thermal screen's U-value in the Hotbox model as a function of air flow rate through the material pores was also studied. To observe the influence of screen porosity on heat loss, the simulation results were given in terms of computed permeability and impermeability. The computed permeability and the experimental U-value were found to be in good agreement on comparing the simulated and experimental U-value results. While forecasting the energy load and evaluating alternative screen performances, it was observed that when using energy-saving screens for the greenhouse energy-saving energy simulation (TRNSYS), the screen's permeability must be considered.

In conclusion, energy-saving screens with material qualities, such as aluminised surface, asymmetry, low IR emissivity, low IR transmittance, low porosity, high IR reflectance, and high thickness would exhibit greater heat resistance. Based on these qualities, such screens can reduce the operational air leakage and energy usage, both ideal properties for preventing excessive heat loss.

## Funding

This work was supported by the Korea Institute of Planning and Evaluation for Technology in Food, Agriculture, Forestry (IPET) through Agriculture, Food and Rural Affairs Convergence Technologies Program for Educating Creative Global Leader, funded by Ministry of Agriculture, Food and Rural Affairs (MAFRA) (717001-7). This research was supported by Basic Science Research Program through the National Research Foundation of Korea (NRF), funded by the Ministry of Education [NRF-2019R1I1A3A01051739].

## Declaration of competing interest

The authors declare that they have no known competing financial interests or personal relationships that could have appeared to influence the work reported in this paper.

## Appendix A. Supplementary data

Supplementary data to this article can be found online at https://doi.org/10.1016/j.biosystemseng.2022.03.002.

## REFERENCES


Abdel-Ghany, A. M., Al-Helal, I. M., Shady, M. R., & Ibrahim, A. A. (2015). Convective heat transfer coefficients between horizontal plastic shading nets and air. *Energy and Buildings, 93*, 119–125. https://doi.org/10.1016/j.enbuild.2015.02.010. October 2017.

Abu Bakar, N. N., Hassan, M. Y., Abdullah, H., Rahman, H. A., Abdullah, M. P., Hussin, F., & Bandi, M. (2015). Energy efficiency index as an indicator for measuring building energy performance: A review. *Renewable and Sustainable Energy Reviews, 44*, 1–11. https://doi.org/10.1016/j.rser.2014.12.018. April.

Ahamed, M. S., Guo, H., & Tanino, K. (2019). Energy saving techniques for reducing the heating cost of conventional greenhouses. *Biosystems Engineering, 178*, 9–33. https://doi.org/10.1016/j.biosystemseng.2018.10.017

Ahamed, M. S., Guo, H., & Tanino, K. (2020). Modeling heating demands in a Chinese-style solar greenhouse using the transient building energy simulation model TRNSYS. *Journal of Building Engineering, 29*, 101114. https://doi.org/10.1016/j.jobe.2019.101114. April 2019.

Akpenpuun, T. D., Na, W. H., Ogunlowo, Q. O., Rabiu, A., Adesanya, M. A., Addae, K. S., Kim, H. T., & Lee, H.-W. (2021). Effect of glazing configuration as an energy-saving strategy in naturally ventilated greenhouses for strawberry (Seolhyang sp.) cultivation. *Journal of Agricultural Engineering, 52*(2), 1–22. https://doi.org/10.4081/jae.2021.1177

Al-Helal, I. M., & Abdel-Ghany, A. M. (2011). Energy partition and conversion of solar and thermal radiation into sensible and latent heat in a greenhouse under arid conditions. *Energy and Buildings, 43*(7), 1740–1747. https://doi.org/10.1016/j.enbuild.2011.03.017

Andersson, N. E. (2010). Properties of thermal screens used for energy saving in greenhouses. In *International conference on agricultural engineering* (pp. 1–6).

Asdrubali, F., Evangelisti, L., Grazieschi, G., & Guattari, C. (2019). Influence of sky temperatures on building energy needs. *Building Simulation Conference Proceedings, 1*, 293–299. https://doi.org/10.26868/25222708.2019.210326

Baeza, E., Hemming, S., & Stanghellini, C. (2020). Materials with switchable radiometric properties: Could they become the perfect greenhouse cover? *Biosystems Engineering, 193*, 157–173. https://doi.org/10.1016/j.biosystemseng.2020.02.012

Baglivo, C., Mazzeo, D., Panico, S., Bonuso, S., Matera, N., Congedo, P. M., & Oliveti, G. (2020). Complete greenhouse dynamic simulation tool to assess the crop thermal well-being and energy needs. *Applied Thermal Engineering, 179*, 115698. https://doi.org/10.1016/j.applthermaleng.2020.115698. July.

Balemans, L. (1989). *Assessment of criteria for energetic effectiveness of greenhouse screen* (Ph.D Dessertation.

Balocco, C., Mercatelli, L., Azzali, N., Meucci, M., & Grazzini, G. (2018). Experimental transmittance of polyethylene films in the solar and infrared wavelengths. *Solar Energy, 165*, 199–205. https://doi.org/10.1016/j.solener.2018.03.011. December 2017.

Baneshi, M., Gonome, H., & Maruyama, S. (2020). Wide-range spectral measurement of radiative properties of commercial greenhouse covering plastics and their impacts into the energy management in a greenhouse. *Energy, 210*, 118535. https://doi.org/10.1016/j.energy.2020.118535

Blonquist, J. M., Tanner, B. D., & Bugbee, B. (2009). Evaluation of measurement accuracy and comparison of two new and three traditional net radiometers. *Agricultural and Forest Meteorology, 149*(10), 1709–1721. https://doi.org/10.1016/j.agrformet.2009.05.015

Castellano, S., Starace, G., De Pascalis, L., Lippolis, M., & Scarascia Mugnozza, G. (2016). Test results and empirical correlations to account for air permeability of agricultural nets. *Biosystems Engineering, 150*, 131–141. https://doi.org/10.1016/j.biosystemseng.2016.07.007

Choab, N., Allouhi, A., Maakoul, A. El, Kousksou, T., Saadeddine, S., & Jamil, A. (2021). Effect of greenhouse design parameters on the heating and cooling requirement of greenhouses in Moroccan climatic conditions. *IEEE Access, 9*, 2986–3003. https://doi.org/10.1109/ACCESS.2020.3047851

Cuce, E., Harjunowibowo, D., & Cuce, P. M. (2016). Renewable and sustainable energy saving strategies for greenhouse systems: A comprehensive review. *Renewable and Sustainable Energy Reviews, 64*, 34–59. https://doi.org/10.1016/j.rser.2016.05.077

De Zwart, H. F. (1996). In *Analyzing energy-saving options in greenhouse cultivation using a simulation model*. the Netherlands: Agricultural University Of Wageningen. PhD Thesis. Ph.D. Dissertation.

Diop, S., Lee, J.-W., Na, W.-H., & Lee, H.-W. (2012). Overall heat transfer coefficient measurement of covering materials with thermal screens for greenhouse using the hot box method. *Journal of The Korean Society of Agricultural Engineers, 54*(5), 1–7. https://doi.org/10.5389/ksae.2012.54.5.001

Feuilloley, P., & Issanchou, G. (1996). Greenhouse covering materials measurement and modelling of thermal properties using the hot box method, and condensation effects. *Journal of Agricultural Engineering Research, 65*(2), 129–142. https://doi.org/10.1006/jaer.1996.0085

Frangi, P., Piatti, R., & Amoroso, G. (2011). Evaluation of different screens for energy saving in the greenhouse. *Acta Horticulturae, 893*, 275–280. https://doi.org/10.17660/actahortic.2011.893.22

Geoola, F., Kashti, Y., Levi, A., & Brickman, R. (2009). A study of the overall heat transfer coefficient of greenhouse cladding materials with thermal screens using the hot box method. *Polymer Testing, 28*(5), 470–474. https://doi.org/10.1016/j.polymertesting.2009.02.006

Hemming, S., Baeza, E., Mohammadkhani, V., & Van Breugel, B. (2017). *Energy saving screen materials* (Vol. 94). https://www.kasalsenergiebron.nl/content/research/20035_Schermprestaties__methode_voor_bepaling_energiebesparing.pdf.

Hung Anh, L. D., & Pásztory, Z. (2021). An overview of factors influencing thermal conductivity of building insulation materials. *Journal of Building Engineering, 44*, 102604. https://doi.org/10.1016/j.jobe.2021.102604

Jones, B., Das, P., Chalabi, Z., Davies, M., Hamilton, I., Lowe, R., Milner, J., Ridley, I., & Shrubsole, C. (2012). In *The relationship between permeability and infiltration in conjoined dwellings. August 2016.*.

Kraniotis, D. (2015). *Dynamic characteristics of wind-driven air infiltration in buildings - the impact of wind gusts under unsteady wind conditions*. https://doi.org/10.13140/RG.2.1.3607.9444. Dynamic characteristics of wind-driven air infiltration in buildings The impact of wind gusts under unsteady wind conditions Dyn (Issue December).

López-Martínez, A., Molina-Aiz, F. D., Valera, D. L., & Espinoza-Ramos, K. E. (2020). Models for characterising the aerodynamics of insect-proof screens from their geometric parameters. *Biosystems Engineering, 192*, 42–55. https://doi.org/10.1016/j.biosystemseng.2020.01.013

López, A., Molina-Aiz, F. D., Valera, D. L., & Peña, A. (2016). Wind tunnel analysis of the airflow through insect-proof screens and comparison of their effect when installed in a

mediterranean greenhouse. *Sensors, 16*(5), 5–8. https://doi.org/10.3390/s16050690

Lu, X., & Memari, A. M. (2018). Comparative study of Hot Box Test Method using laboratory evaluation of thermal properties of a given building envelope system type. *Energy and Buildings, 178*, 130–139. https://doi.org/10.1016/j.enbuild.2018.08.044

Mashonjowa, E., Ronsse, F., Milford, J. R., & Pieters, J. G. (2013). Modelling the thermal performance of a naturally ventilated greenhouse in Zimbabwe using a dynamic greenhouse climate model. *Solar Energy, 91*, 381–393. https://doi.org/10.1016/j.solener.2012.09.010

Miguel, A. F. (1998). Airflow through porous screens: From theory to practical considerations. *Energy and Buildings, 28*(1), 63–69. https://doi.org/10.1016/S0378-7788(97)00065-0

Miguel, A. F., Van De Braak, N. J., & Bot, G. P. A. (1997). Analysis of the airflow characteristics of greenhouse screening materials. *Journal of Agricultural Engineering Research, 67*(2), 105–112. https://doi.org/10.1006/jaer.1997.0157

Ogunlowo, Q. O., Akpenpuun, T. D., Na, W. H., Rabiu, A., Adesanya, M. A., Addae, K. S., Kim, H. T., & Lee, H. W. (2021). Analysis of heat and mass distribution in a single-and multi-span greenhouse microclimate. *Agriculture, 11*(9), 891. https://doi.org/10.3390/agriculture11090891

Ouazzani Chahidi, L., Fossa, M., Priarone, A., & Mechaqrane, A. (2021). Energy saving strategies in sustainable greenhouse cultivation in the mediterranean climate – a case study. *Applied Energy, 282*, 116156. https://doi.org/10.1016/j.apenergy.2020.116156. PA.

Papadakis, G., Briassoulis, D., Scarascia Mugnozza, G., Vox, G., Feuilloley, P., & Stoffers, J. A. (2000). Radiometric and thermal properties of, and testing methods for, greenhouse covering materials. *Journal of Agricultural Engineering Research, 77*(1), 7–38. https://doi.org/10.1006/jaer.2000.0525

Rafiq, A. (2019). *Measurement of longwave radiative properties of energy saving greenhouse screens* (Measurement of Longwave Radiative Properties of Energy Saving Greenhouse Screens. December.

Rafiq, A., Na, W. H., Rasheed, A., Kim, H. T., & Lee, H. W. (2019). Determination of thermal radiation emissivity and absorptivity of thermal screens for greenhouse. *Protected Horticulture and Plant Factory, 28*(4), 311–321. https://doi.org/10.12791/KSBEC.2019.28.4.311

Rafiq, A., Na, W. H., Rasheed, A., Kim, H. T., & Lee, L. (2020). Measurement of convective heat transfer coefficients of horizontal thermal screens under natural conditions. *Protected Horticulture and Plant Factory, 29*(1), 9–19. https://doi.org/10.12791/KSBEC.2020.29.1.9

Rafiq, A., Na, W. H., Rasheed, A., Lee, J. W., Kim, H. T., & Lee, H. W. (2021). Measurement of longwave radiative properties of energy-saving greenhouse screens. *Journal of Agricultural Engineering, 52*(3). https://doi.org/10.4081/jae.2021.1209 [in this issue].

Rasheed, A., Kwak, C. S., Kim, H. T., & Lee, H. W. (2020). Building energy an simulation model for analyzing energy saving options of multi-span greenhouses. *Applied Sciences, 10*(19), 1–23. https://doi.org/10.3390/app10196884

Rasheed, A., Kwak, C. S., Na, W. H., Lee, J. W., Kim, H. T., & Lee, H. W. (2020). Development of a building energy simulation model for control of multi-span greenhouse microclimate. *Agronomy, 10*(9). https://doi.org/10.3390/agronomy10091236

Rasheed, A., Lee, J. W., & Lee, H. W. (2015). A review of greenhouse energy management by using building energy simulation. *Protected Horticulture and Plant Factory, 24*(4), 317–325. https://doi.org/10.12791/ksbec.2015.24.4.317

Rasheed, A., Lee, J. W., & Lee, H. W. (2018a). Development of a model to calculate the overall heat transfer coefficient of greenhouse covers. *Spanish Journal of Agricultural Research, 15*(4), Article e0208. https://doi.org/10.5424/sjar/2017154-10777

Rasheed, A., Lee, J. W., & Lee, H. W. (2018b). Development and optimization of a building energy simulation model to study the effect of greenhouse design parameters. *Energies, 11*(8), 2001. https://doi.org/10.3390/en11082001

Rasheed, A., Lee, J. W., & Lee, H. W. (2018c). Evaluation of overall heat transfer coefficient of different greenhouse thermal screens using building energy simulation. *Protected Horticulture and Plant Factory, 27*(4), 294–301. https://doi.org/10.12791/ksbec.2018.27.4.294

Santolini, E., Pulvirenti, B., Torreggiani, D., & Tassinari, P. (2019). Novel methodologies for the characterization of airflow properties of shading screens by means of wind-tunnel experiments and CFD numerical modeling. *Computers and Electronics in Agriculture, 163*, 104800. https://doi.org/10.1016/j.compag.2019.05.009. January.

SCL. (2018). *Trnsys 18* (Vol. 3). Solar Energy Laboratory, Univ. of Wisconsin-Madison. http://www.trnsys.com/.

Sherman, M. H., & Chan, R. (2004). *Building airtightness: Research and practice*. Lawrence Berkeley National Library. Report No. LBNL -53356. https://www.researchgate.net/publication/238573993_Building_Airtightness_Research_and_Practice.

Solar Energy Laboratory. (2018). *Trnsys 18 manual, documentation, vols. 4,5 & 7* (Vol. 3). Solar Energy Laboratory, Univ. of Wisconsin-Madison. http://www.trnsys.com/.

Teitel, M., Barak, M., & Antler, A. (2009). Effect of cyclic heating and a thermal screen on the nocturnal heat loss and microclimate of a greenhouse. *Biosystems Engineering, 102*(2), 162–170. https://doi.org/10.1016/j.biosystemseng.2008.11.013

Valera, D. L., Álvarez, A. J., & Molina, F. D. (2006). Aerodynamic analysis of several insect-proof screens used in greenhouses. *Spanish Journal of Agricultural Research, 4*(4), 273–279. https://doi.org/10.5424/sjar/2006044-204

Vitoshkin, H., Barak, M., Shenderey, C., Haslavsky, V., & Arbel, A. (2019). Improving greenhouse insulation through multilayer thermal screens using the hot box method. *Proceedings of the World Congress on Mechanical, Chemical, and Material Engineering*, 8–11. https://doi.org/10.11159/htff19.124

Vitoshkin, H., Haslavsky, V., Barak, M., Ziffer, E., & Arbel, A. (2021). Numerical and experimental investigation of heat transfer across semi-transparent horizontal screen layers. *Journal of Building Engineering, 42*(March), 103082. https://doi.org/10.1016/j.jobe.2021.103082

Yano, A., & Cossu, M. (2019). Energy sustainable greenhouse crop cultivation using photovoltaic technologies. *Renewable and Sustainable Energy Reviews, 109*(April), 116–137. https://doi.org/10.1016/j.rser.2019.04.026

Zhang, S., Guo, Y., Zhao, H., Wang, Y., Chow, D., & Fang, Y. (2020). Methodologies of control strategies for improving energy efficiency in agricultural greenhouses. *Journal of Cleaner Production, 274*, 122695. https://doi.org/10.1016/j.jclepro.2020.122695

Zhang, K., Mcdowell, T. P., & Kummert, M. (2017). Sky temperature estimation and measurement for longwave radiation calculation polytechnique montréal , dept . of mechanical engineering , montréal , QC , Canada thermal energy system specialists , LLC , madison , WI , USA abstract modelling longwave heat. *Building Simulation, 3*, 2093–2102.